

Phase Transitions: A Multinational Journal

Publication details, including instructions for authors and subscription information:

<http://www.tandfonline.com/loi/gpht20>

Slow molecular processes in a nematic liquid crystal confined to random porous network formed by aerosil particles

M. Rajeswari^a, S. Dhara^a, K. Venu^b, V.S.S. Sastry^a & R. Dabrowski^c

^a School of Physics, University of Hyderabad, Hyderabad 500 046, Andhra Pradesh, India

^b Soctrionics Technologies Pvt. Ltd, Hyderabad 500 034, Andhra Pradesh, India

^c Institute of Chemistry, Military University of Technology, 00-908 Warsaw, Poland

Available online: 16 Feb 2012

To cite this article: M. Rajeswari, S. Dhara, K. Venu, V.S.S. Sastry & R. Dabrowski (2012): Slow molecular processes in a nematic liquid crystal confined to random porous network formed by aerosil particles, Phase Transitions: A Multinational Journal, 85:4, 322-336

To link to this article: <http://dx.doi.org/10.1080/01411594.2011.646269>

PLEASE SCROLL DOWN FOR ARTICLE

Full terms and conditions of use: <http://www.tandfonline.com/page/terms-and-conditions>

This article may be used for research, teaching, and private study purposes. Any substantial or systematic reproduction, redistribution, reselling, loan, sub-licensing, systematic supply, or distribution in any form to anyone is expressly forbidden.

The publisher does not give any warranty express or implied or make any representation that the contents will be complete or accurate or up to date. The accuracy of any instructions, formulae, and drug doses should be independently verified with primary sources. The publisher shall not be liable for any loss, actions, claims, proceedings,

demand, or costs or damages whatsoever or howsoever caused arising directly or indirectly in connection with or arising out of the use of this material.

Slow molecular processes in a nematic liquid crystal confined to random porous network formed by aerosil particles

M. Rajeswari^{a*}, S. Dhara^a, K. Venu^b, V.S.S. Sastry^a and R. Dabrowski^c

^aSchool of Physics, University of Hyderabad, Hyderabad 500 046, Andhra Pradesh, India;

^bSocronics Technologies Pvt. Ltd, Hyderabad 500 034, Andhra Pradesh, India; ^cInstitute of Chemistry, Military University of Technology, 00-908 Warsaw, Poland

(Received 20 November 2011; final version received 25 November 2011)

Frequency dispersion measurements of proton spin–lattice relaxation rates (R_1) of liquid crystal 4-propyl-4'-pentylazoxybenzene in bulk and confined samples (in random porous network of aerosil nano-particles) are reported in isotropic and nematic phases. Significant low-frequency increase in R_1 in confined samples indicates slow molecular reorientations mediated by translational displacements near the adsorbing porous surface. The resulting dispersion behavior of R_1 ($\sim \omega^{-p}$) reflects the nature of the random surface ($p = 0.5$ for equi-partition of the diffusive modes). The observed temperature-independent exponent in the isotropic phase ($p = 0.34$) indicates the abundance of low-wavelength surface modes. Its temperature-dependent higher values in the nematic phase (from 0.59 to 0.65 on cooling), and increased spin–lattice coupling via this mechanism, show progressive onset of longer wavelength modes. A detailed analysis shows the effect of confinement on the order director fluctuations, molecular reorientations, and translational diffusion of the molecules.

Keywords: liquid crystals; porous media; RMTD process; molecular dynamics; NMR relaxometry

1. Introduction

Interest in liquid crystalline materials confined to various types of geometries expanded greatly in the last two decades because of their important role in electro-optic devices and physical properties, which require basic understanding of surface–fluid interactions. Independent of the methods used to confine the liquid crystals (LCs), these systems have one underlying common theme: a symmetry-breaking, non-planar confinement imposed by the surrounding matrix. In addition, confined LCs differ significantly from macroscopic bulk systems because of their large surface-to-volume ratio. Their composite nature profoundly affects the ordering of the LC molecules and their susceptibility to external fields, making them ideal for electro-optic applications [1].

Among the confined LC systems, LC-aerosil dispersions are demonstrated to be particularly interesting to study through many distinct experimental and theoretical methodologies [2–17]. While porous matrices like nucleopore, anopore, millipore, and controlled porous glass (CPG) all have a well-defined geometry of the pores, aerosil, and

*Corresponding author. Email: raji.hcu@gmail.com

aerogel systems in contrast provide random porous structures. Aerosil gels are partly similar to silica aerogel, a different type of fractal silica gel used to confine LC. Aerosil and aerogel systems are nearly identical in several aspects: fractal-like nature of the gel structure, surface composition, chemical properties, as well as density. The crucial difference between the two systems is their differing response to elastic strains since aerogels possess much larger shear modulus than aerosil gels. In LC-aerogel systems, the silica network is fixed in space and the elastic strains imposed by the random anchoring surfaces are fully quenched. The disorder introduced by even the low-density aerogels is so severe that the features of phase transitions are dramatically smeared [16]. In contrast, in aerosil gels, a weaker, better-controlled random disorder can be introduced: elastic strains can be partially annealed, thus reducing some of the disordering effects. In addition, the ability to grow a network directly within the LC permits the formation of structures of higher porosity [17,18]. Indeed, a distinct advantage of aerosil systems is the ease of producing nearly arbitrary silica densities.

Nuclear magnetic relaxation methods, widely used to probe molecular dynamics in many condensed systems, are extremely sensitive to the orientational order of molecules and have the potential to report on the dynamic processes over a wide time scale [19]. The random network confining the LC induces ordering near the surface, which decreases exponentially with a correlation length depending on the disordering density. For example, the deuterium NMR studies on the LC 8CB confined to aerosil matrix [6,9] revealed the details of the director configuration and the orientational order in the voids, supporting this scenario. The proton NMR relaxometry in this context provides a valuable supplementing technique, which throws further light on the degree of surface-induced order and on the changes in the molecular dynamics induced upon confinement [14,15].

In this article, we present a detailed dispersion study of proton spin–lattice relaxation rates in bulk 4-propyl-4'-pentylazoxybenzene (PPA) and PPA confined to aerosil matrix at two different concentrations. These relaxation rates of confined systems are found to be very sensitive in the presence of the silica network, and show qualitatively different frequency dependence compared to the bulk sample. We analyze the additional contribution to the relaxation rate on confinement, in terms of slow reorientation of molecules very near the porous surfaces due to adsorption kinetics. This article is organized as follows: the experimental details are given in Section 2. The relaxation models and the analysis of the experimental data are discussed in Sections 3 and 4. The last section summarizes the results of this work.

2. Experimental details

The LC PPA was synthesized in the laboratories in Warsaw, Poland. The molecular structure and its phase sequence are shown in Figure 1. The LC–aerosil mixtures were prepared by the solvent method [3]. Aerosil (type A300 from Degussa Corp.) was initially dried over-night at 200°C under vacuum before adding to a dilute solution of the LC in pure acetone. This solution was kept in the sonicator for over 2 h to achieve a homogeneous dispersion. The solvent was then evaporated by keeping the sample at 60°C for over 15 h. The mixture was then transferred into an NMR tube and was sealed under vacuum. Aerosil A300 consists of small silica spheres of diameter 7 nm and a specific surface area of 300 m² g⁻¹. The surface of these spheres is covered with hydroxyl groups that interact with each other via hydrogen bonding, and the resulting system thus forms a 3-D random network. Due to the hydrophilic nature of the spheres and the polar nature of

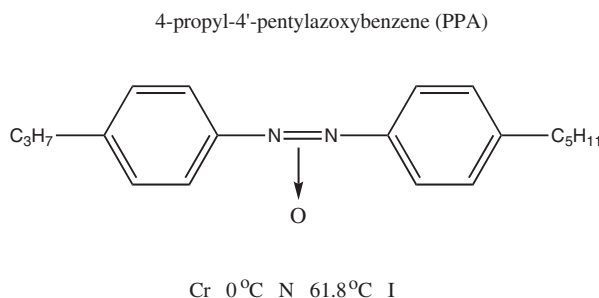


Figure 1. Molecular structure and phase sequence of the liquid crystal PPA.

the LC, the alignment of the molecules at the silica surfaces is homeotropic. The density of silica particles in our samples was 0.05 (Sample A) and 0.07 g cm⁻³ (Sample B). The shift of the isotropic-to-nematic transition temperature (T_{NI}) is within ± 1 K at both the aerosil concentrations.

Proton spin–lattice relaxation rates (R_1) were measured over a range of Larmor frequencies using the field-cycling NMR relaxometry (Stelar Spinmaster FFC 2000) from 10 kHz to 10 MHz and a pulsed variable field spectrometer at 20 MHz. The decay of the observed magnetization was exponential over several decades of the observation time, indicating single relaxation time constant. The errors in the R_1 measurements were within 3% and the temperature of the sample was controlled to ± 0.1 K. The frequency dependence of these rates in bulk and confined PPA systems (at two different concentrations) in the isotropic and nematic phases are shown in Figure 2(a–c). Their temperature dependences at different Larmor frequencies (in bulk and confined samples) are shown in Figure 3(a–c). These plots bring out clearly the pre-transitional behavior near the nematic–isotropic point, and also portray specific features of the different phases in the bulk as well as in confined LC systems.

3. Relaxation models

The proton spin–lattice relaxation is mediated via the time modulation of dipole–dipole interactions between the neighboring spins [19,20], effected through various molecular processes characteristic of the liquid crystalline systems. It is customary to assume their statistical independence, and hence express the observed relaxation rate R_{1T} as a sum of individual contributions $\{R_1\}_i$, as

$$R_{1T} = \sum_i \{R_1\}_i, i = R, SD, CF, OPF, ODF, \text{ and } RMTD \quad (1)$$

where the summation index i covers different molecular mechanisms, like: local molecular reorientations (R), translational self-diffusion (SD), orientational order critical fluctuations (CF), order parameter fluctuations (OPF), order director fluctuations (ODF), and rotations/reorientations mediated by translational displacements (RMTD).

In the case of LC molecules, the molecular reorientations about their long and short axes can be distinguished due to separated time scales: reorientations around the long axes are fast on the typical NMR experimental time scale and hence give a frequency-independent contribution. On the other hand, dynamics about the short axes are slow, and could fall in the time window of the experiment. The relaxation rate contribution due to

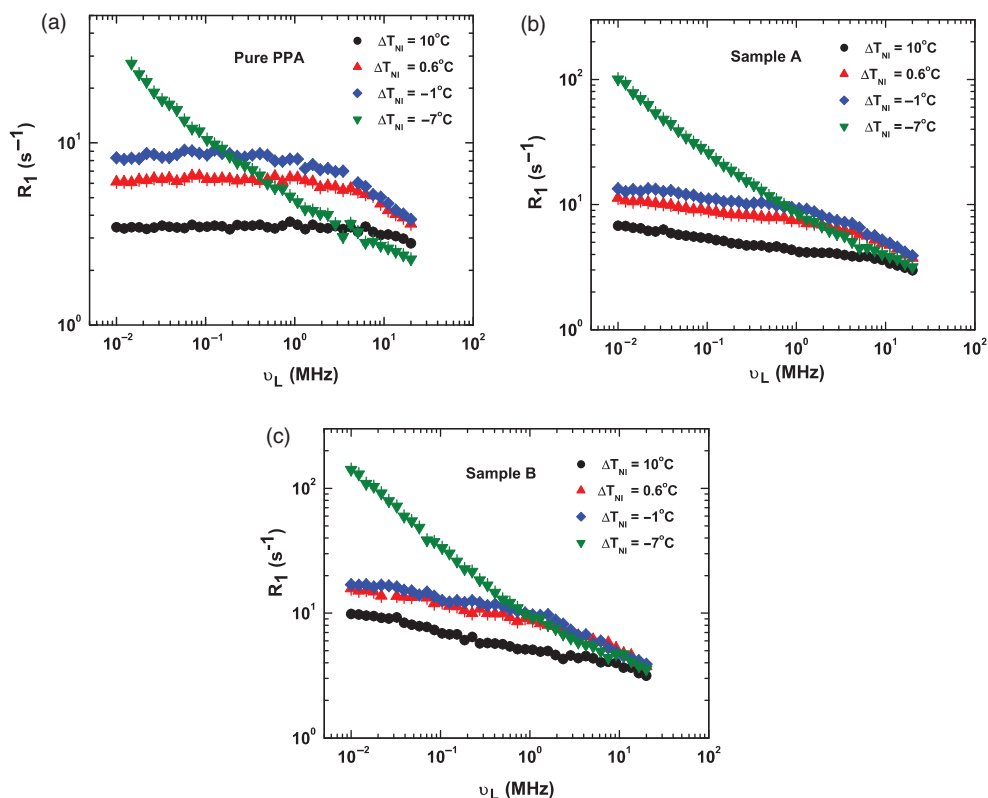


Figure 2. Frequency dispersions of proton spin–lattice relaxation rate R_1 for PPA in the bulk (a), in Sample A (b), and in Sample B (c) in the isotropic and nematic phases.

these reorientations is given by the well-known BPP expression [21], which depends on a correlation time τ_R and a pre-factor A_R . The translational self-diffusion modulates the intermolecular spin interactions and its contribution to the total relaxation rate in the isotropic phase was calculated analytically [22] and later extended to the liquid crystalline phases [23,24]. This contribution primarily depends on the diffusion coefficient D and a related pre-factor A_D .

The collective processes observed in LC systems are critical fluctuations of the orientational order just above the nematic–isotropic transition (T_{NI}), order parameter fluctuations just below this transition, and order director fluctuations in the nematic phase. The first of these contributions arises from the time-modulation of the dipolar interactions due to short-range nematic order fluctuations [19], and is quantified by a correlation time τ_{CF} and a pre-factor A_{CF} . In contrast to short-range nematic order fluctuations in the isotropic phase, fluctuations in the magnitude of the nematic order parameter S are effective in relaxing the nuclear spins just below nematic–isotropic transition [19]. Order director fluctuations observed in the nematic phase are typically characterized by a spin–lattice relaxation rate that depends on frequency as $R_1 \sim \omega^{-1/2}$. However, this characteristic frequency dependence is modified in the limiting cases of both high- and low-frequency cut-off values. The relaxation rate becomes independent below a lower cut-off frequency and it varies as $R_1 \sim \omega^{-2}$ above an upper cut-off frequency.

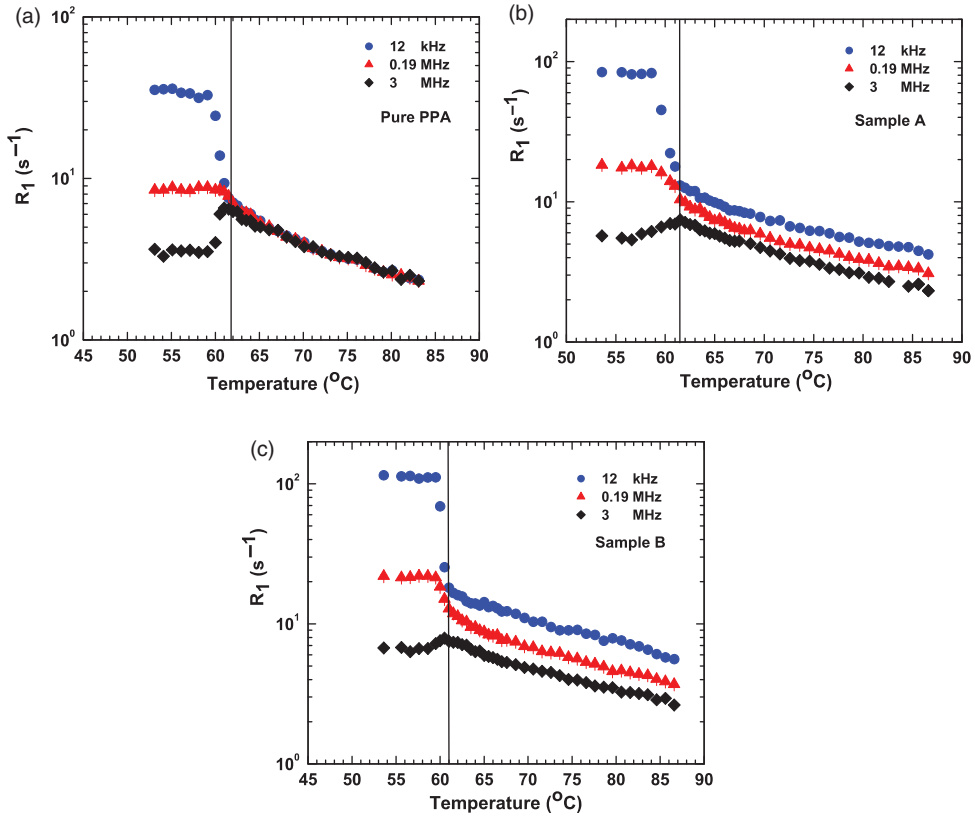


Figure 3. Temperature dependences of proton spin–lattice relaxation rate R_1 for PPA in the bulk (a), in Sample A (b), and in Sample B (c) in the isotropic and nematic phases.

The pre-factor A_{ODF} and the cut-off frequencies associated with ODF depend on the temperature, nematic order parameter S , and visco-elastic properties of the liquid crystalline medium [19].

In the case of LCs confined to nanometer size cavities, the molecular rotations and translational displacements close to the cavity surfaces are restricted, and are affected by the influence of the surface. Such constrained dynamics was observed in many LC systems confined to different types of random porous matrices [14,15,25–28], and the underlying rotational processes are referred to as RMTD. The translational displacements close to the surface is analyzed in terms of diffusion modes with different wave numbers q , decaying in time with damping constant $\tau_q = 1/Dq^2$. The relaxation rate for this mechanism is the sum of all diffusion modes taking into account that each mode might contribute with a different weight. The weights depend on the structure of the confined porous matrix, and in general the orientational structure factor quantifying their relative importance is a complex function of the wave number. But in some cases, it can be approximated by a power law with an exponent p . Therefore the spin–lattice relaxation rate associated with this mechanism for an arbitrary value of the exponent p was calculated as [28]

$$(R_1)_{\text{RMTD}} = A_{\text{RMTD}} \left\{ \frac{1}{\omega^p} \int_{z_{\min}}^{z_{\max}} \frac{z^3 - zp}{1 + z^4} dz + \frac{1}{(2\omega)^p} \int_{z_{\min}/\sqrt{2}}^{z_{\max}/\sqrt{2}} \frac{z^3 - zp}{1 + z^4} dz \right\} \quad (2)$$

where $z_{\min} = (\omega_{\text{RMTDmin}}/\omega)^{1/2}$ and $z_{\max} = (\omega_{\text{RMTDmax}}/\omega)^{1/2}$. A_{RMTD} is a pre-factor depending on the diffusion coefficient, geometrical features of the confined matrix, and residual dipole–dipole proton–spin interaction. The frequencies ω_{RMTDmin} and ω_{RMTDmax} are the lower and higher cut-off limits, and are related to the largest and smallest molecular displacements l_{\max} and l_{\min} of a molecule through the following relation: $\omega_{\text{RMTDmin}} = l_{\max}^2/4D$ and $\omega_{\text{RMTDmax}} = l_{\min}^2/4D$. Apart from the additional RMTD contribution in the nano-confined samples, all the other relaxation mechanisms are common for both the bulk and confined systems.

4. Analysis and discussion

The spin–lattice relaxation rate profiles in different phases of the LCs are analyzed in terms of the above-mentioned different relaxation mechanisms. The parameters quantifying these processes were evaluated by employing a non-linear least square fitting procedure based on the Levenberg–Marquardt (LM) algorithm [29]. The broad objective of this regression analysis is to locate efficiently the region of parameter space which is best suited to account for the experimental data according to the chosen model, and then minimize the deviation (mean square error, χ^2) between the experimental and computed results, based on maximum likelihood criterion. The LM algorithm combines the gradient search method with parabolic approximation by modifying exclusively the diagonal components of the Jacobian (curvature) matrix associated with the model during the gradient search, and asymptotically withdrawing these modifications in the immediate neighborhood of the χ^2 minimum, to recover the parabolic approximation. Further simplification results by considering only the linearized version of the Jacobian matrix. This analysis is carried out under these conditions, and the errors in the fitted parameters thus obtained are to be taken as indicative (particularly if there are significant correlations among some of them). To reduce the complexity of the fitting procedure, we used experimentally measured values, wherever available, as inputs for the model parameters.

4.1. Isotropic phase

The relaxation rate dispersions of the bulk PPA at higher temperatures ($\Delta T_{\text{NI}} = T - T_{\text{NI}} = 10^\circ\text{C}$ and 15°C) in the isotropic phase are well described by a superposition of the two relevant relaxation mechanisms: molecular reorientations (R) and translational self-diffusion (SD). We made use of the reported value of diffusion constant D of a related azoxybenzene [30] in analyzing the present data, noting that bulk properties of diffusion in the isotropic phase of such similar systems are very much comparable. We found that the coupling constant A_{D} has not varied significantly over the temperature range (within the estimated errors) in the isotropic phase; so its average value was used at all temperatures in this phase. The reorientational correlation time τ_{R} has been found to increase with the decrease of temperature, while its strength A_{R} decreased. Close to the phase transition, i.e., at $\Delta T_{\text{NI}} = 0.6^\circ\text{C}$, 2°C , and 6°C , a better fit to the experimental data was obtained with an additional mechanism, taking into account the critical fluctuations of the orientational order (CF) in addition to the R and SD. The correlation time τ_{CF} and the strength of the interaction A_{CF} were found to increase on approaching the transition from above. The observed behavior of all these parameters (with respect to frequency and temperature) is very much comparable to the earlier observations reported in typical bulk LC samples. The fitted experimental data at 10°C and 0.6°C away from T_{NI} are shown in

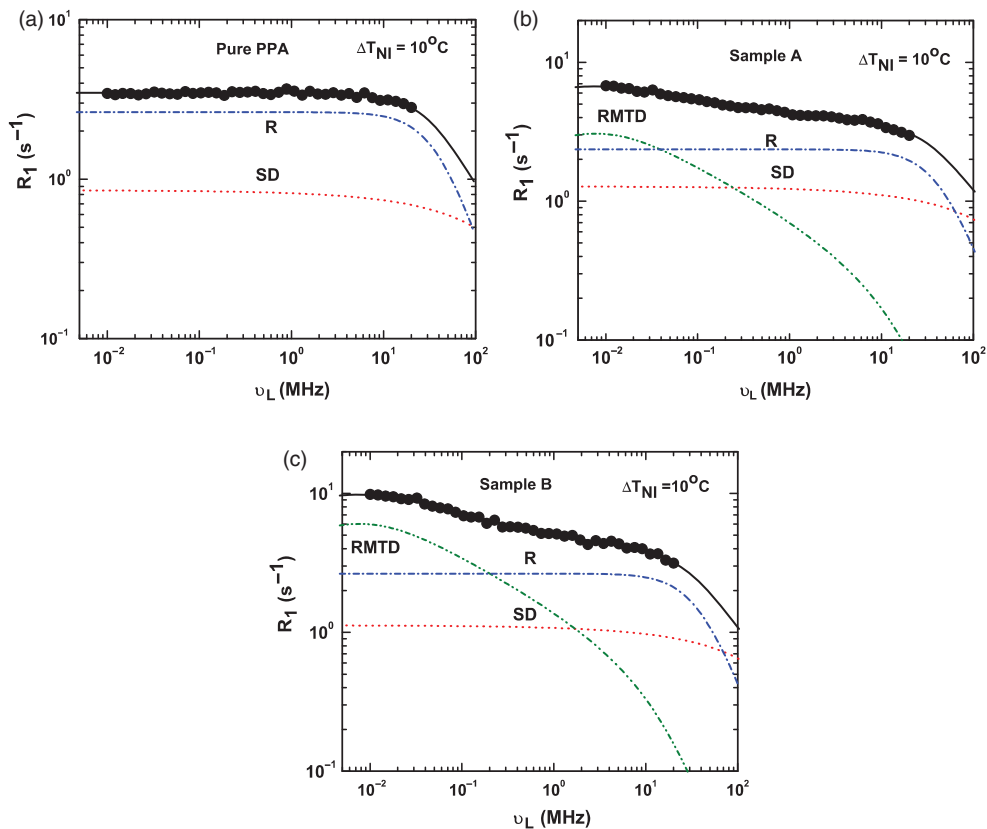


Figure 4. (color online) Frequency dispersion of the proton spin–lattice relaxation rate R_1 of PPA at $\Delta T_{NI} = 10^\circ\text{C}$: in the bulk (a), Sample A (b), and Sample B (c). The solid line represents the calculated total relaxation rate obtained by fitting the experimental data to the theoretical models explained in Section 3. The dashed (color lines) lines represent the corresponding relaxation mechanisms. The fit parameters are given in Table 1.

Figures 4 and 5, respectively, and the associated parameters at different temperatures are presented in Table 1.

The relative increase in the relaxation rate in the confined systems (particularly in the low-frequency region) can be consistently explained by invoking the RMTD mechanism, and the corresponding dispersion data were fitted by including this process also. The analysis clearly indicates the dominant role of RMTD below 1 MHz. It exhibits a characteristic power law frequency dependence between the two cut-off regimes, $(R_1)_{\text{RMTD}} \propto \omega^{-p}$, with $p = 0.34 \pm 0.05$, which is different from the other reported confined systems [27,28]. The deviation of p from its equi-partition value (0.5) signals the important contribution of low wavelength diffusion modes in this phase of the system. It may be noted that our recent work on 8OCB confined to identical environment also yielded almost the same value of p within errors of estimation [15]. It appears that practically identical confining environment provided for two different LCs is leading to a very similar distribution of diffusive modes, thereby clearly alluding to the strong possibility that the observed power law is essentially arising from the underlying structure factor of the (random) porous surfaces. Changes in the cut-off frequencies of the RMTD mechanism

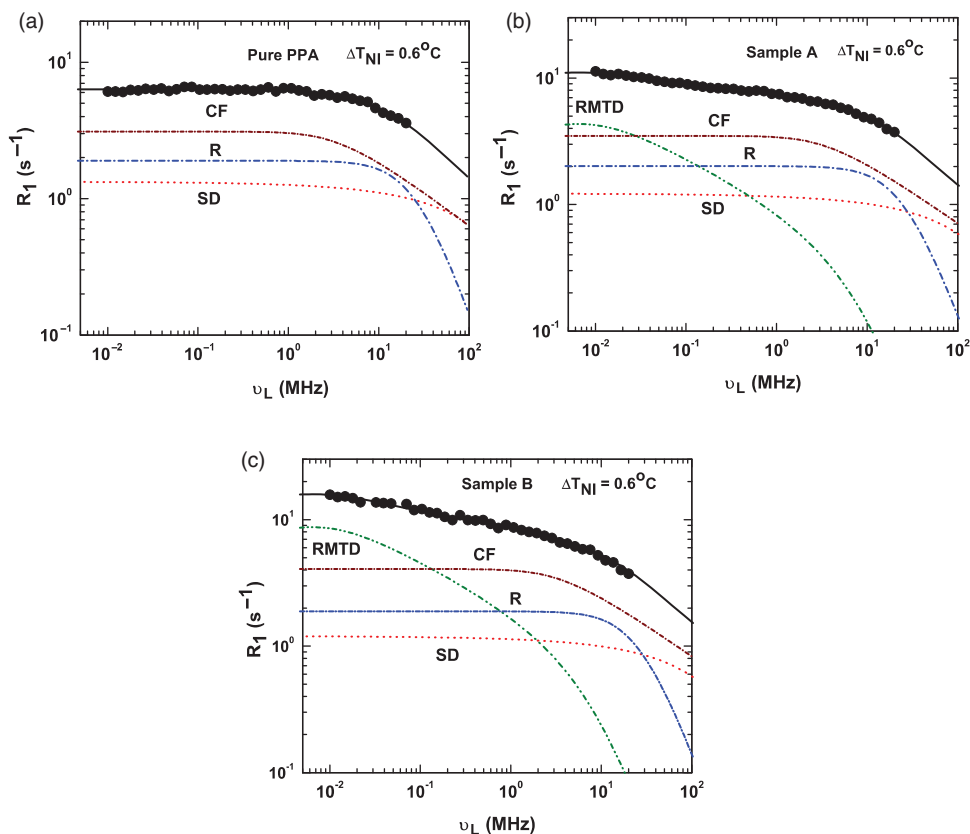


Figure 5. (color online) Frequency dispersion of the proton spin–lattice relaxation rate R_1 of PPA at $\Delta T_{NI} = 0.6^\circ\text{C}$: in the bulk (a), Sample A (b), and Sample B (c). The solid line represents the calculated total relaxation rate obtained by fitting the experimental data to the theoretical models explained in Section 3. The dashed (color lines) lines represent the corresponding relaxation mechanisms. The fit parameters are given in Table 1.

with the decrease in temperature are manifestations of the decrease in the diffusion coefficient on cooling, and are in turn associated with the largest and smallest molecular displacements near the surface (l_{\max} and l_{\min}) that could cause significant loss in the correlation of molecular orientations. The experimental data on PPA report rather a nominal change in l_{\min} , steadily increasing from about 1.5 nm to 2 nm over 15°C (Figure 6). In comparison, in the case of 8OCB, for a similar variation of temperature above its T_{NI} value, it is observed that l_{\min} is comparable (~ 1.5 nm) at $\Delta T_{NI} = 15^\circ\text{C}$, but increases to about 9 nm very close to T_{NI} . Further, its variation with temperature in 8OCB appears to approximate to a power law, unlike PPA. This contrasting variation of l_{\min} in these two LC systems, with a confining matrix having very similar structure factor (i.e., very close p values), brings about an interesting point for discussion. The larger value of l_{\min} near the transition, and its apparent pre-transitional behavior, in the case of 8OCB are indicative of the presence of significant ordering near the surface, relative to PPA [15]. In addition, this length scale is fairly insensitive to temperature in the present system. Taking into account the fact that both the systems seem to need RMTD mechanism for interpretation of their data in the isotropic phase (thus confirming observable adsorption

Table 1. Best fit parameters in the bulk and confined PPA at two different concentrations in the isotropic phase.

Sample	Bulk PPA						Sample A						Sample B						
	15	10	10	6	10	0.6	15	10	15	6	2	0.6	15	10	15	6	2	0.6	
ΔT_{NI} (°C)							18.5	15	10	15	13.9	10	15	10	18	13.2	10	15	9
A_D 10^8 s ⁻²							(3.8)	(2.9)	(2.9)	(1)	(0.78)	(0.3)	(2)	(1.1)	(2)	(1.1)	(0.2)	(0.5)	(0.3)
D 10^{-11} m ² s ⁻¹	18	15	12.5	10.5	9.6	0.6	18	15	15	12.5	10.5	9.6	18	15	18	15	12.5	10.5	9.6
A_R 10^9 s ⁻²	1.20	1.22	0.94	0.8	0.54	0.54	1.2	1.22	1.22	0.94	0.8	0.54	1.2	1.22	1.2	0.94	0.8	0.54	0.54
τ_R 10^{-9} s	(0.02)	(0.03)	(0.04)	(0.01)	(0.02)	(0.02)													
τ_R 10^{-9} s	1.71	2.16	2.27	3.0	3.4	3.4	1.24	1.97	2.19	2.19	3.26	3.72	1.29	2.2	2.27	3.27	3.49	3.49	3.49
A_{CF} 10^3 s ^{-3/2}	(0.01)	(0.06)	(0.14)	(0.1)	(0.23)	(0.23)	(0.22)	(0.01)	(0.11)	(0.03)	(0.03)	(0.09)	(0.01)	(0.1)	(0.06)	(0.1)	(0.09)	(0.1)	(0.09)
τ_{CF}/OPF 10^{-9} s																			
A_{CF} 10^3 s ^{-3/2}																			
τ_{CF}/OPF 10^{-9} s																			
A_{RMTD} 10^2 s ^{-(1+p)}	-																		
$\omega_{RMTDmin}/2\pi$ kHz																			
$\omega_{RMTDmax}/2\pi$ MHz																			
P																			

Note: Error estimates are given in parentheses.

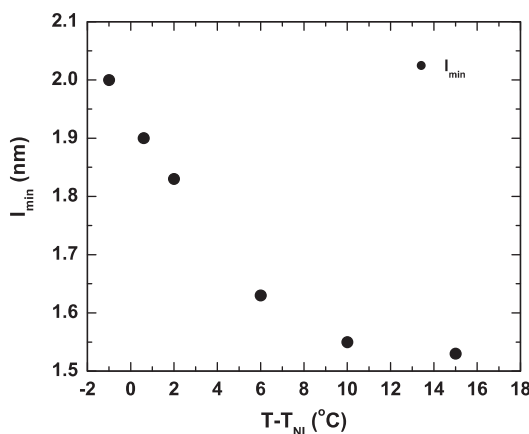


Figure 6. Variation of l_{min} with the temperature in the isotropic phase.

effects in both the cases), we attribute this dissimilar behavior with respect to l_{min} to the difference in the orientations of the dipoles on the two molecules vis-à-vis the aligning direction preferred by the local structure due to the anchoring interactions. The strength of this interaction A_{RMTD} shows an Arrhenius behavior with temperature in both the LCs, the associated activation energy with this process being about 35 kJ mole^{-1} for both the samples. This seems to provide another pointer to the qualitative difference in the surface interactions of the two LC systems.

4.2. Nematic phase

The dispersion profiles in the nematic phase of PPA in bulk as well as in confined samples are discussed in this section, focusing first on the nematic phase, very near to the transition temperature ($\Delta T_{NI} = T - T_{NI} = -1^\circ\text{C}$), where order parameter fluctuations are known to provide the dominant mechanism for relaxation in the bulk samples (Figure 7). By analyzing the data based on this mechanism [19], the characteristic time associated with these fluctuations τ_{OPF} is estimated to be about 134 ns. The effect of confinement at this temperature, relative to the bulk sample, is interesting. There is practically no change in τ_R due to confinement in PPA remaining at about 3 ns, while it changes from 8.14 to 5.4 ns in 8OCB. This observation seems to be interestingly correlated to the exponent p in the power law governing the frequency dependence between the corresponding frequency limits, $\omega_{RMTDmin}$ and $\omega_{RMTDmax}$. The exponent in the nematic phase of the confined PPA system remains the same (at ~ 0.34) as in the isotropic phase for PPA, while it shows a perceptible increase in the confined 8OCB on the onset of the nematic phase (from 0.39 in the isotropic phase to 0.45 just below the transition). Common to 8OCB and PPA is the observation that progressive confinement (i.e., from Sample A to Sample B) leads in both the systems, an increased coupling to the lattice via the RMTD mechanism (namely, A_{RMTD} increases with network density in these samples) [31].

We now discuss the results of our analysis at three temperatures deep in the nematic phase ($\Delta T_{NI} = -3^\circ\text{C}$, -7°C , and -10°C). In the bulk sample (Table 2), τ_R decreases progressively on cooling due to the gradual increase in the orientational order in the sample. Within the frequency range of the experiment, no leveling of the relaxation rate

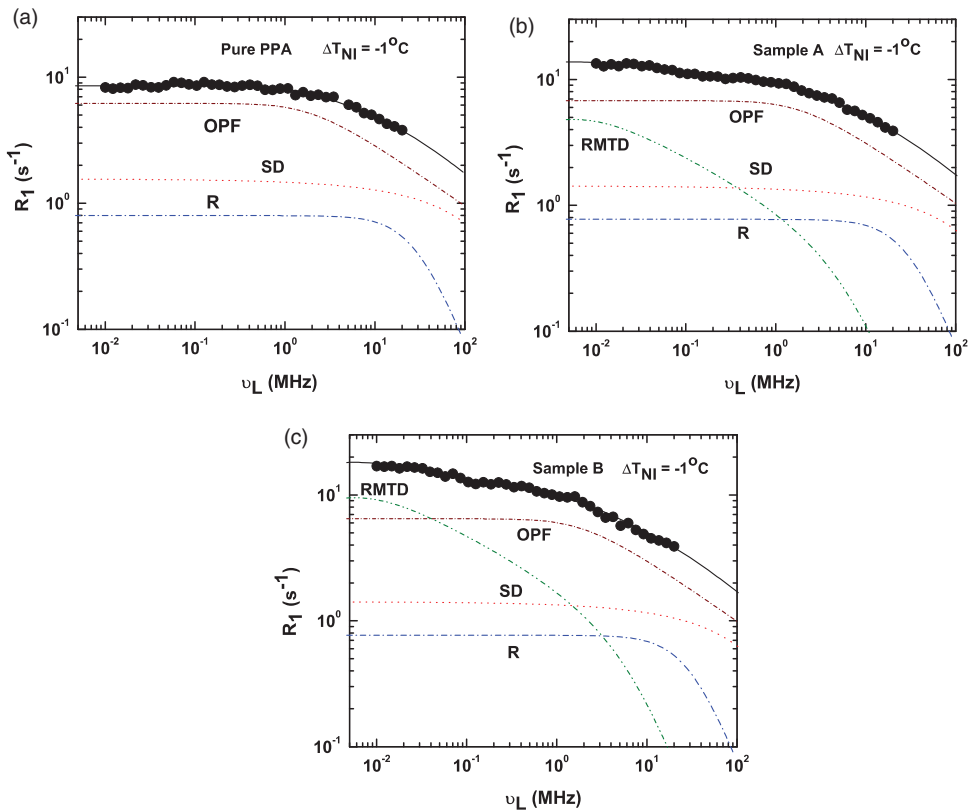


Figure 7. (Color online) Frequency dispersion of the proton spin–lattice relaxation rate R_1 of PPA at $\Delta T_{\text{NI}} = -1^\circ\text{C}$: in the bulk (a), Sample A (b), and Sample B (c). The solid line represents the calculated total relaxation rate obtained by fitting the experimental data to the theoretical models explained in Section 3. The dashed (color lines) lines represent the corresponding relaxation mechanisms. The fit parameters are given in Table 2.

(i.e., reaching a plateau) at low-frequency end could be observed, indicating that ω_{ODFmin} should be significantly below the lowest frequency studied. A_{ODF} , representing the coupling of the spin system to the lattice via ODF, marginally increases initially on cooling and saturates at $\Delta T_{\text{NI}} = -10^\circ\text{C}$ (Table 2).

Effect due to confinement on the dynamic parameters of the PPA at these temperatures of the nematic phase is summarized in Table 2, and Figure 8 shows the contribution of different relaxation mechanisms at $\Delta T_{\text{NI}} = -7^\circ\text{C}$. One immediate discernible effect of confinement is the significant increase of ω_{ODFmin} to the range of MHz. The confinement due to the aerosil 3-D network seems to be placing a severe restriction on the long-wavelength ODF modes, pushing the value of the corresponding cut-off frequency by an order of magnitude. This circumstance leaves room for other slow mechanisms, like RMTD, to play their visible role at much lower frequencies. An interesting consequence of confinement on PPA system is that the exponent p changes from 0.34 (within the vicinity of the transition $\Delta T_{\text{NI}} = -1^\circ\text{C}$) to 0.63. This is of course an indication of the qualitative changes in the effective structure factor probed by the diffusing molecules, signaling a change, on cooling, to a regime where long wavelength diffusive modes are more probable.

Table 2. Best fit parameters in the bulk and confined PPA at two different concentrations in the nematic phase.

Sample	Bulk PPA				Sample A				Sample B			
	-1	-3	-7	-10	-1	-3	-7	-10	-1	-3	-7	-10
ΔT_{NI} ($^{\circ}\text{C}$)	10	10	5	4	9.1	17.1	11.7	9.9	9.1	19	14.5	12.4
A_D 10^8 s^{-2}					(0.4)	(0.1)	(0.08)	(0.1)	(0.4)	(0.1)	(0.02)	(0.1)
D $10^{-11} \text{ m}^2/\text{s}$	8.2	6.8	5.5	4.6	8.2	6.8	5.5	4.6	8.2	6.8	5.5	4.6
A_R 10^9 s^{-2}	0.26	0.38	0.5	0.56	0.26	0.38	0.5	0.56	0.26	0.38	0.5	0.56
τ_R 10^{-9} s	3.03	3.23	2.52	2.23	2.98	3.23	2.52	2.23	2.95	3.23	2.52	2.23
A_{OPF} $10^3 \text{ s}^{-3/2}$	(0.07)	(0.01)	(0.04)	(0.03)								
A_{OPF} $10^3 \text{ s}^{-3/2}$	(0.59)	(0.16)	(0.04)	(0.16)	26.2				24.98			
τ_{OPF} 10^{-9} s	23.9											
A_{ODF} $10^3 \text{ s}^{-3/2}$	(2.11)				134.1				134.1			
$\omega_{ODF_{\text{min}}}/2\pi \text{ kHz}$	134.1											
$\omega_{ODF_{\text{min}}}/2\pi \text{ kHz}$	(11.22)	6.49	6.98	6.98	6.49	6.49	6.98	6.98	6.49	6.49	6.98	6.98
$\omega_{ODF_{\text{max}}}/2\pi \text{ MHz}$		(0.04)	(0.03)	(0.04)								
A_{RMTD} $10^2 \text{ s}^{-(1+p)}$		1	1	1								
$\omega_{RMTD_{\text{min}}}/2\pi \text{ kHz}$		100	100	100								
$\omega_{RMTD_{\text{max}}}/2\pi \text{ MHz}$					0.6	159.1	284.6	301	1.18	161	548	669.8
P					(0.01)	(21.77)	(21.11)	(1.77)	(0.02)	(0.89)	(3.72)	(4)
					13	1	1	1	13	1	1	1
					15	8.43	6.35	6.82	15	13	6	6.5
					(0.6)	(0.69)	(0.46)	(0.31)	(0.6)	(1.2)	(0.6)	(0.5)
					0.34	0.6	0.63	0.63	0.34	0.6	0.65	0.66
					(0.05)	(0.01)	(0.006)	(0.01)	(0.05)	(0.01)	(0.01)	(0.02)

Note: Error estimates are given in parentheses.

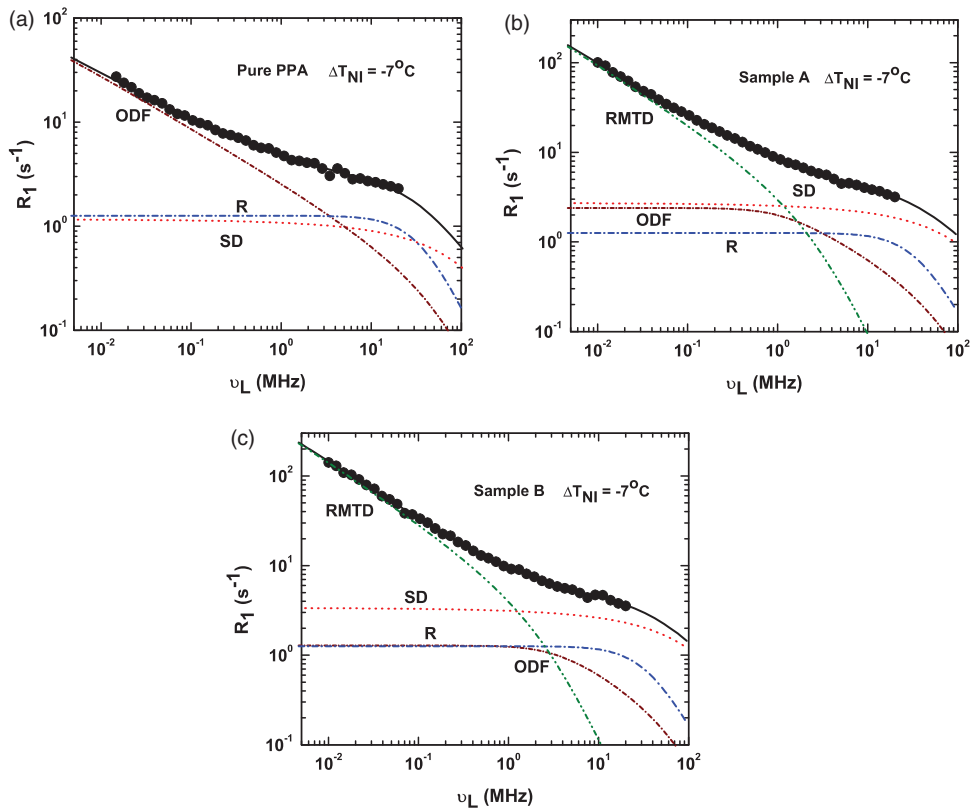


Figure 8. (Color online) Frequency dispersion of the proton spin–lattice relaxation rate R_1 of PPA at $\Delta T_{NI} = -7^\circ\text{C}$: in the bulk (a), Sample A (b), and Sample B (c). The solid line represents the calculated total relaxation rate obtained by fitting the experimental data to the theoretical models explained in Section 3. The dashed (color lines) lines represent the corresponding relaxation mechanisms. The fit parameters are given in Table 2.

A similar change was observed in the case of 8OCB on confinement ($p = 0.58$) [31], and in other such systems. In the case of CPG matrix, however, with confining lengths in the range of ~ 15 nm, the distinguishing features of the phase transition were smeared out and the exponent was observed to increase continuously [28]. In this case, the exponent however increases marginally in the deep nematic phase. The difference between these two cases suggests that the exponent value in the present system is limited by pore size. Finally, the progressive onset of the orientational order on cooling into the nematic phase has profound effect in the confined samples. The effect, for example, on $\omega_{ODF_{\min}}$ and A_{RMTD} is seen in both the samples (A and B), correspondingly more in Sample B.

5. Conclusions

We present the frequency dispersions of spin–lattice relaxation rates at various temperatures covering the isotropic and nematic phases of LC PPA, and compare the results obtained in the bulk sample with two confined systems with different average pore sizes. In the isotropic phase, PPA exhibits pre-transitional effects on the relaxation profiles

within a range of about 6–7°C above T_{NI} , like in the case of a typical LC. Surface interactions of the LC medium as a result of confinement induce RMTD mechanism, which provides an insight into the surface topology (in terms of its orientational structure factor) and adsorption kinetics (ω_{RMTD} cut-off values). We find that the exponent p obtained from confined PPA samples is lower than the equi-partition value (0.5), and is essentially the same as was reported by 8OCB under essentially identical random environment. The observed value (0.34–0.38) is indicative of the relative abundance of low-wavelength diffusion modes, reflecting the nature of the surface formed by the 3-D network of the chosen aerosil particles. Temperature variation of l_{min} in the isotropic phase of PPA is compared with confined 8OCB. The observed qualitative difference seems to be related to the difference in the direction of the dipoles located on the two molecules (relative to the respective long axis) and hence the observed differing sensitivity to decoherence effects on diffusion. The effect of increasing orientational order on cooling the nematic PPA, and confinement related effects at each of the temperatures in this phase, are qualitatively analyzed. The lower cut-off frequency of the ODF mechanism is observed to shift to higher frequencies, yielding to RMTD mechanism to play a dominant role at low frequencies even in this phase. This mechanism has been observed to be more effective in the nematic phase (by an order of magnitude) relative to its isotropic phase.

Acknowledgments

M. Rajeswari would like to thank the University Grants Commission (UGC), New Delhi, for providing financial support under the RFSMS scheme.

References

- [1] G.P. Crawford and S. Zumer, *Liquid Crystals in Complex Geometries*, Taylor and Francis, London, 1996.
- [2] G.A. Puchkovskaya, Y.A. Reznikov, A.A. Yakubov, O.V. Yaroshchuk, and A.V. Glushchenko, *Transformation of hydrogen bonding of a liquid crystal–aerosil system under the influence of an electric field*, J. Mol. Struct. 381 (1996), pp. 133–139.
- [3] B. Zhou, G.S. Iannacchione, C.W. Garland, and T. Bellini, *Random-field effects on the nematic–smectic-A phase transition due to silica aerosil particles*, Phys. Rev. E 55 (1997), pp. 2962–2968.
- [4] G.S. Iannacchione, C.W. Garland, J.T. Mang, and T.P. Rieker, *Calorimetric and small angle X-ray scattering study of phase transitions in octylcyanobiphenyl–aerosil dispersions*, Phys. Rev. E 58 (1998), pp. 5966–5981.
- [5] A. Hourri, T.K. Bose, and J. Thoen, *Effect of silica aerosil dispersions on the dielectric properties of a nematic liquid crystal*, Phys. Rev. E 63 (2001), pp. 051702–517026.
- [6] T. Jin and D. Finotello, *Aerosil dispersed in a liquid crystal: Magnetic order and random silica disorder*, Phys. Rev. Lett. 86 (2001), pp. 818–821.
- [7] T. Bellini, L. Radzihovsky, J. Toner, and N.A. Clark, *Universality and scaling in the disordering of a smectic liquid crystal*, Science 294 (2001), pp. 1074–1079.
- [8] P.S. Clegg, C. Stock, R.J. Birgeneau, C.W. Garland, A. Roshi, and G.S. Iannacchione, *Effect of a quenched random field on a continuous symmetry breaking transition: Nematic to smectic-A transition in octyloxycyanobiphenyl–aerosil dispersions*, Phys. Rev. E 67 (2003), p. 021703.
- [9] T. Jin and D. Finotello, *Controlling disorder in liquid crystal aerosil dispersions*, Phys. Rev. E 69 (2004), p. 041704.
- [10] A. Roshi, G.S. Iannacchione, P.S. Clegg, and R.J. Birgeneau, *Evolution of the isotropic-to-nematic phase transition in octyloxycyanobiphenyl+aerosil dispersions*, Phys. Rev. E 69 (2004), p. 031703.

- [11] M. Caggioni, A. Roshi, S. Barjami, F. Mantegazza, G.S. Iannacchione, and T. Bellini, *Isotropic to nematic transition of aerosil-disordered liquid crystals*, Phys. Rev. Lett. 93 (2004), p. 127801.
- [12] G. Sinha, J. Leys, C. Glorieux, and J. Thoen, *Dielectric spectroscopy of aerosil-dispersed liquid crystal embedded in anopore membranes*, Phys. Rev. E 72 (2005), p. 051710.
- [13] A. Roshi, S. Barjami, G.S. Iannacchione, D. Paterson, and I. McNulty, *Structure and dynamics of a nanocolloidal silica gel dispersion*, Phys. Rev. E 74 (2006), p. 031404.
- [14] E. Anoardo, F. Grinberg, M. Vilfan, and R. Kimmich, *Proton spin-lattice relaxation in a liquid crystal-aerosil complex above the bulk isotropization temperature*, Chem. Phys. 297 (2004), pp. 99–110.
- [15] M. Rajeswari, S. Dhara, K. Venu, V.S.S. Sastry, and R. Dbrowski, *Slow molecular processes in a liquid crystal embedded in aerosil matrix: Nuclear magnetic relaxometric study*, Mol. Cryst. Liq. Cryst. 546 (2011), pp. 45–56.
- [16] H. Zeng, B. Zalar, G.S. Iannacchione, and D. Finotello, *Effects of quenched disorder on the orientational order of the octylcyanobiphenyl liquid crystal*, Phys. Rev. E 60 (1999), pp. 5607–5618.
- [17] S. Park, R.L. Leheny, R.J. Birgeneau, J.L. Gallani, C.W. Garland, and G.S. Iannacchione, *Hydrogen-bonded silica gels dispersed in a smectic liquid crystal: A random field XY system*, Phys. Rev. E 65 (2002), p. 050703.
- [18] G.S. Iannacchione, *Review of liquid-crystal phase transitions with quenched random disorder*, Fluid Phase Equilibria 222–223 (2004), pp. 177–187.
- [19] R.Y. Dong, *Nuclear Magnetic Resonance of Liquid Crystals*, 2nd ed., Springer-Verlag, Berlin, 1997.
- [20] A. Abragam, *The Principles of Nuclear Magnetism*, Clarendon Press, Oxford, 1961.
- [21] N. Bloembergen, E.M. Purcell, and R.V. Pound, *Relaxation effects in nuclear magnetic resonance absorption*, Phys. Rev. 73 (1948), pp. 679–712.
- [22] H.C. Torrey, *Nuclear spin relaxation by translational diffusion*, Phys. Rev. 92 (1953), pp. 962–969.
- [23] S. Zumer and M. Vilfan, *Theory of nuclear spin relaxation by translational self-diffusion in liquid crystals: Nematic phase*, Phys. Rev. A 17 (1978), pp. 424–433.
- [24] M. Vilfan and S. Zumer, *Theory of nuclear-spin relaxation by translational self-diffusion in liquid crystals: Smectic A phase*, Phys. Rev. A 21 (1980), pp. 672–680.
- [25] R. Kimmich and H. Werner Weber, *NMR relaxation and the orientational structure factor*, Phys. Rev. B 47 (1993), pp. 11788–11794.
- [26] R. Kimmich and E. Anoardo, *Field-cycling NMR relaxometry*, Prog. Nucl. Magn. Reson. Spectrosc. 44 (2004), pp. 257–320.
- [27] P.J. Sebastiao, D. Sousa, A.C. Ribeiro, M. Vilfan, G. Lahajnar, J. Seliger, and S. Zumer, *Field-cycling NMR relaxometry of a liquid crystal above T_{NI} in mesoscopic confinement*, Phys. Rev. E 72 (2005), p. 061702.
- [28] M. Vilfan, T. Apih, P.J. Sebastiao, G. Lahajnar, and S. Zumer, *Liquid crystal 8CB in random porous glass: NMR relaxometry study of molecular diffusion and director fluctuations*, Phys. Rev. E 76 (2007), p. 051708.
- [29] W.H. Press, B.P. Flannery, S.A. Teukolsky, and W.T. Vetterling, *Numerical Recipes: The Art of Scientific Computation*, Cambridge University Press, Cambridge, 1986.
- [30] M. Cifelli, G. Cinacchi, and L. De Gaetani, *Smectic order parameters from diffusion data*, J. Chem. Phys. 125 (2006), p. 164912.
- [31] M. Rajeswari, S. Dhara, K. Venu, V.S.S. Sastry, and R. Dabrowski, *NMR relaxometry study of a liquid crystal 8OCB confined to random porous matrix* (to be published).